Correlation between acoustic emission distribution and stress variation through the depth of RC beam cross sections

LIU Simeng[1,2], Matthew R. Pearson[3], Mark Eaton[3], Rhys Pullin[3]

1. State Key Laboratory Breeding Base of Mountain Bridge and Tunnel Engineering (Chongqing Jiaotong University) , Chongqing, P.R.China

2. School of Civil Engineering, Chongqing Jiaotong University, Chongqing, P.R.China

3. Cardiff School of Engineering, Cardiff University, Cardiff, Wales, UK

Highlights

- The acoustic emission distribution through the depth of RC beam sections is studied.
- AE parameters can characterise behaviours of RC beams in the depth direction.
- AE event intensity shows a higher correlation than energy-based parameters in the study.
- The correlation between AE and stress responses was demonstrated to be very strong.
- A new option for estimating stress levels in engineering and science is considered.

Abstract

Two established techniques for monitoring concrete under loading are Acoustic Emission (AE) and strain gauges. The distribution of strain, along with that of stress, on a beam cross section is well established both theoretically and experimentally. However, the AE distribution through the depth of the cross section has received little attention previously. In addition, the correlation between the AE distribution and that of stress on the section could provide valuable insight into the condition of a structure. Therefore, these topics are experimentally addressed in this article. Specifically, six Reinforced Concrete (RC) beams were tested. AE and Digital Image Correlation (DIC) were employed to monitor the beams during loading. Finally, the AE and stress distributions were analysed. The results showed that AE parameters are capable of characterising behaviours of RC beams in the depth direction. Furthermore, the distribution of AE events strongly correlated with that of compressive stress, especially

in the post-reinforcement yielding stage. According to these findings, it is highly possible to estimate stress levels of RC beam structures in engineering and science by adopting the AE technique.

Keywords
Acoustic Emission, Reinforced Concrete, compressive stress distribution, event intensity, absolute energy, signal strength.

1 Introduction

Reinforced Concrete (RC) is one of the most extensively used materials in infrastructure, including bridges, dams, tunnels and buildings. These structures are exposed to deterioration or damage in service due to overloading, ageing, corrosion, fatigue, and environmental hazards, etc. Acoustic Emission (AE) is a non-invasive and passive Non-Destructive Testing (NDT) approach. AE may be defined as the transient elastic waves that are generated by the rapid release of energy from damage sources within a material [1]. AE techniques have been applied to damage diagnosis in civil engineering for decades, for example, on RC structures [2-7], pre-stressed concrete (PC) structures [8-11], glass fibre reinforced composite bridge decks [12] and constructions strengthened with carbon fibre reinforced polymer (CFRP) [13-17]. Compared with other methods, AE techniques have distinctive features. For instance, developing cracks can be located [18].

AE-related concrete research has been carried out for decades, and includes

55 concrete crack classification, damage assessment and non-destructive monitoring. Hu, et
56 al. [5], investigated concrete crack propagation using AE techniques to determine the
57 initial load, crack propagation and final concrete structure failure. Rouchier, et al. [19],
58 used two parameters, the number and amplitude distribution of AE signals, to assess
59 cracking damage. Mohamed, et al. [20], studied the use of AE acquired during loading
60 as a substitute for conventional deformation measurements to assess the integrity of PC
61 beams. Ohtsu and Mori, et al. [21], compared the total number of AE hits with a
62 phenomenological model of steel embedded in concrete subjected to marine
63 environments, and showed that the two curves are in a remarkable agreement. Jochen
64 [22] presented a new concept of automatic AE three-dimensional source localization
65 based on developments from geodesy and ideas from seismology. Vishnuvardhan, et al
66 [23], characterised the sensitivity of active-sensing acousto-ultrasound-based Structural
67 Health Monitoring (SHM) techniques with respect to damage detection, and identified
68 the parameters that influence their sensitivity. The studies discussed above have shown
69 that AE parameters can be related to damage variables/indices, different failure
70 mechanisms and corrosion loss for steel in RC beams.
71 More work specifically linked to this investigation. Vidya, et al. [24] focused on
72 evaluating stress levels according to AE measurements. The researchers conducted an

73 experimental study on the Kaiser effect at different stress levels on RC beams. Fu, et al.
74 [25], investigated if the Kaiser effect exists in both the Brazilian and bending tests, and
75 found that the cumulative AE events vs. stress curves are more suitable for AE
76 investigations than the cumulative AE energy vs. stress curve. Lehtonen, et al. [26],
77 explored the variety of geological and mechanical factors involved in in-situ rock stress
78 estimations, and concluded that stress measurement via the Kaiser Effect-based methods
79 is only likely to be successful if it is supported by key geological and other stress
80 measurement information. Tuncay and Obara [27] compared stress values obtained from
81 AE and the compact conical-ended borehole overcoming techniques, and found that in
82 some stages, the stress values obtained in AE tests were two or three times greater than
83 those obtained by the latter. In conclusion, many practitioners have linked common AE
84 parameters to stress via the Kaiser effect.
85 According to the literature reviewed in this paper, it is evident that the distribution
86 of AE through a cross section of a structure has so far received little attention; hence, we
87 carried out this investigation. This study also carefully examined the possible
88 correlation between the AE distribution and the stress distribution through the depth of
89 an RC beam.
90

2 Fundamental aims

The Mechanics of Materials shows that strain develops linearly through the cross sections of a structure under loading (e.g. Figure 1(a)). In addition, according to the stress-strain relation of concrete (Figure 1(b)), different strain values correspond to different stress magnitudes (Figure 1(c)), meaning that the pattern of the stress distribution on the sections is deterministic and changes with load magnitudes. If the magnitude of the load is sufficient, cracking occurs. Finally, well established research [21, 28-33] has revealed that events, such as cracking, cause the release of energy in materials, forming elastic waves, i.e. AE. Therefore, the following two questions are considerably interesting in science and engineering:

1) How does the AE response vary through the cross sections?

2) What relations between AE and stress may exist during loading on the RC beam structure to failure?

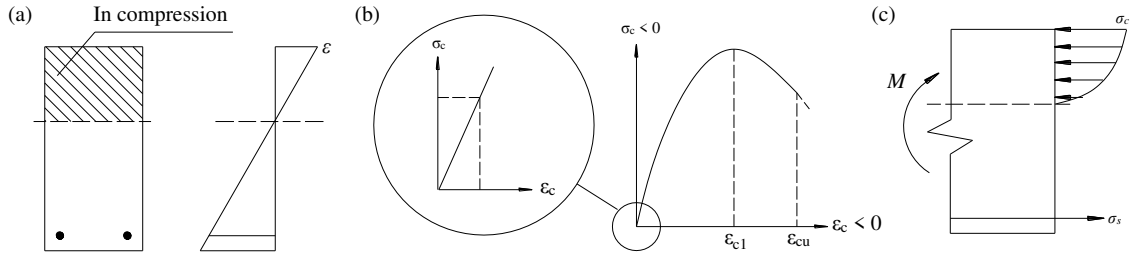

Figure 1. (a) A typical theoretical distribution of strain on an RC beam cross section; (b)

a stress-strain curve of the concrete material [34]; (c) the corresponding stress diagram across the section.

Accordingly, in this study, six RC beams were tested, and the relationship between stress/strain levels and AE signal properties were investigated. The primary attention was paid to the possible correlations between structural and AE response distributions through a RC beam cross section. Figure 2 presents the classic AE parameters used to describe waveforms and perform characterisation of signals [24]. Meanwhile, a new term, called the AE event intensity, was introduced and was referred to the number of AE events acquired per unit area.

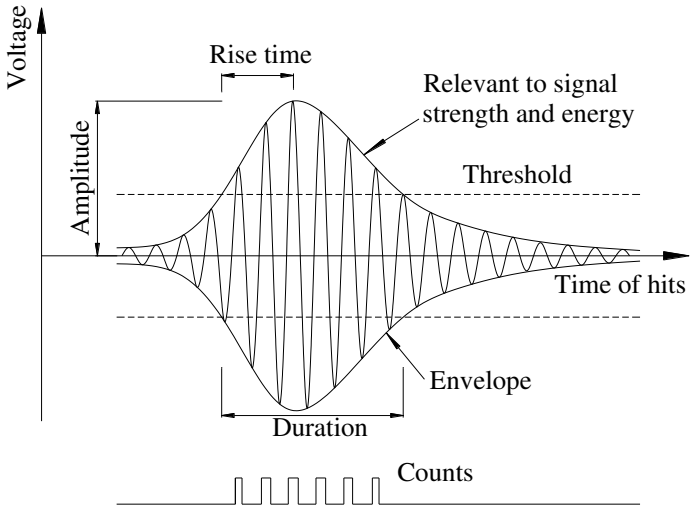

Figure 2. Important AE-related concepts discussed in this paper.

121 # 3 Experiment setup

122 ## *3.1 Experimental specimens*

123 Six RC beam specimens were tested in this study. The beams were cut from a previous
124 experiment. All specimens were carefully examined before being tested in this study to
125 make sure that no severe damage had occurred.

126 The details of these specimens are shown in Figure 3 and Table 1. The sections of
127 all beams are rectangular, 120mm wide and 150mm or 155mm deep, with a clear span
128 of 620 mm (Table 1). In every specimen, one steel bar (N1), 12 mm in diameter, is
129 provided as tensile reinforcement, and another bar (N2), 6 mm in diameter, is used as
130 compressive reinforcement. Stirrups (N3), 6 mm in diameter, are placed at 50 mm c/c
131 distance to avoid shear failure. The beams were designed in accordance with British
132 Standard for grade C40, and the mixture proportion of the concrete was that cement :
133 fine aggregate : coarse aggregate : water = 1:2:3:0.5, by weight. Steel fibres, 30mm or
134 60mm long, were mixed in the concrete, with a ratio of 1% or 2% (by weight), to obtain
135 the Steel Fibre Concrete (SFC). The specimens were cast in a specially made wooden
136 mould and a standard steel mould, and compacted using a needle vibrator.

137

138 **Table 1.** The dimensions, materials and test results of all six RC specimens

No.	Sectional sizes/mm Height x Width	Material	Strength/kN	Failure mode

Beam 1	155x120	SFC ,2%, 30mm	83.41	Bending failure
Beam 2	150x120	Concrete, C40	68.12	Shear failure
Beam 3	150x120	Concrete, C40	68.05	Bending failure
Beam 4	155x120	SFC ,1%, 60mm	85.20	Bending failure
Beam 5	155x120	SFC ,1%, 60mm	79.62	Bending failure
Beam 6	155x120	SFC ,2%, 30mm	82.43	Bending failure

To promote the failure of every beam at its mid-span, a 10 mm deep notch was made. After they were tested, Beams 5 and 6 were cut in half at the failed positions, and the depths of crushed concrete and the lengths of major cracks were then measured.

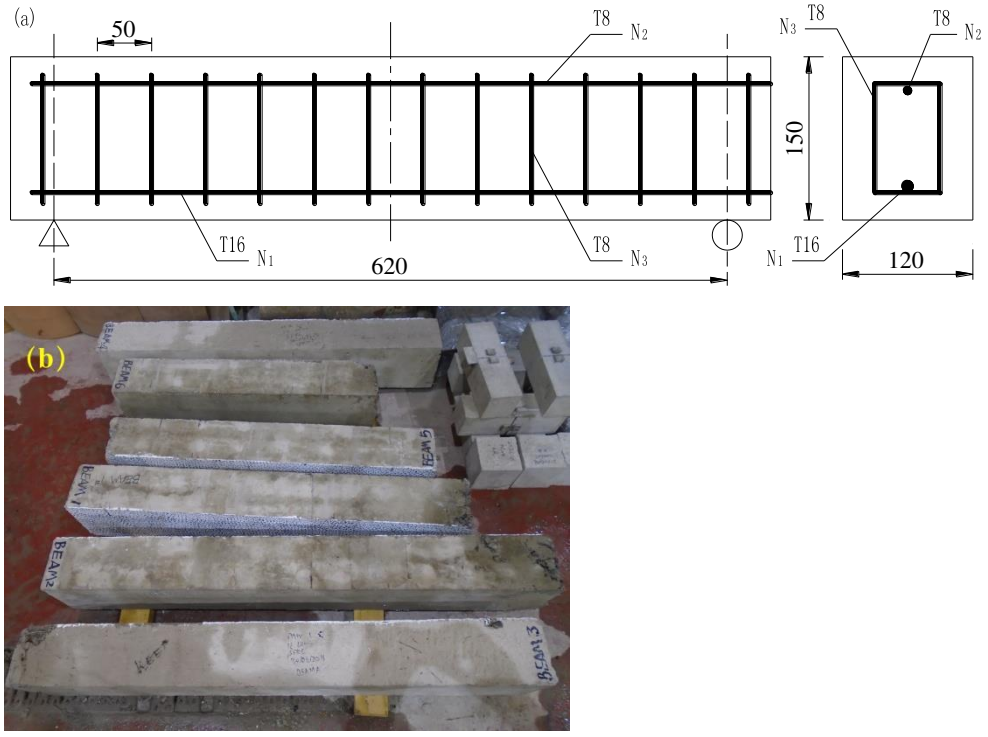

Figure 3. (a) The design details of the simply supported RC beams tested in the study (Units in mm), (b) a photo of all specimens.

149 ***3.2 Instrumentation***

150 AE signals were recorded with a MISTRAS system. The system consisted of
151 preamplifiers (40dB), R6D sensors (40–100 kHz) and a personal computer (PC) with
152 eight AE channels. A full suite of the AEWin software was installed on the PC. The
153 acquisition parameters adopted in the study are listed in Table 2.

154

155 **Table 2.** The parameters used during AE data acquisition.

Parameter	Value
Threshold	45 dB
Velocity	4030 m/s
Hit definition time (HDT)	800 ms
Peak definition time (PDT)	200 ms
Hit lockout time (HLT)	1000 ms

156

157 As stated by Swit [35], since AE signals are mainly registered by sensors that are
158 close enough to the sources of AE events, all sensors were therefore placed around the
159 most probable site of damage – the notch and the pure bending region. Hence, as shown
160 in Figure 4, six sensors (S1 through S6) are mounted on the top and the bottom of every
161 beam. Brown grease was used as an acoustic couplant. Sensor S5 is placed adjacent to
162 each pre-cut notch. In order to make sure all sensors were mounted correctly, a
163 Pencil-Lead Breaks (PLBs) [36] test was completed prior to testing.

164

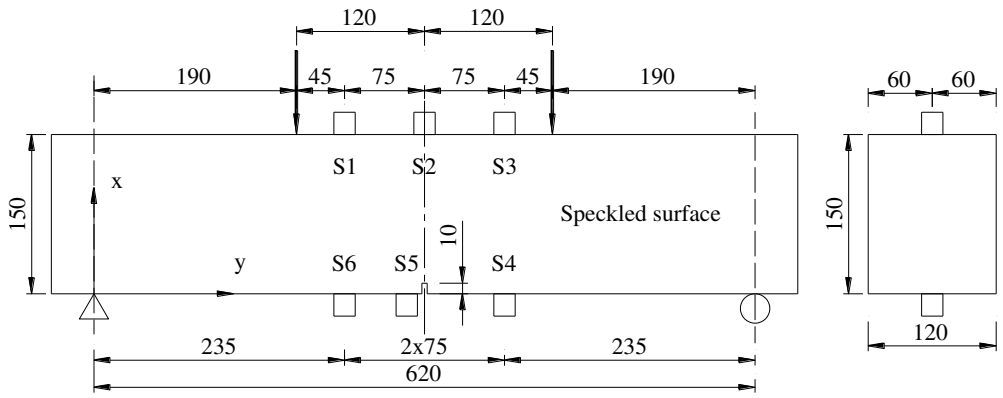

S1 ~ S6 : Acoustic Emission Sensor 1 to 6.

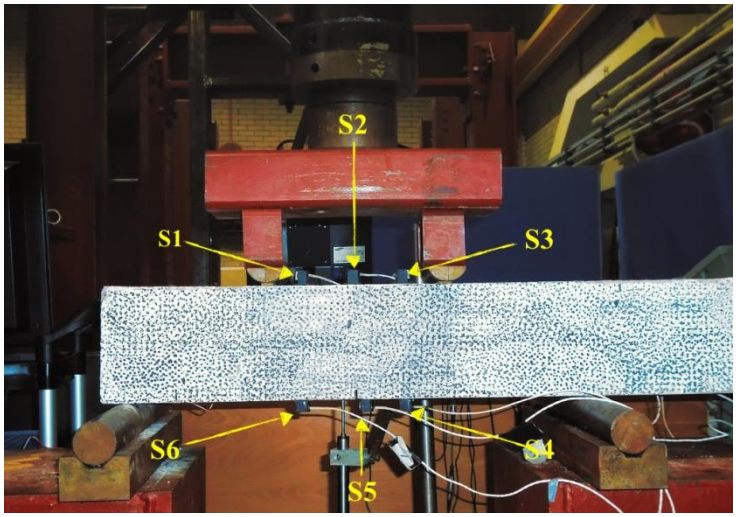

Figure 4. The layout of all six AE sensors employed in tests (Units in mm).

Other instruments used in the study included a digital image correlation (DIC) system, strain gauges and displacement transducers. In order to estimate the strain distribution on a side surface of each RC beam, DIC was employed. The area of interest on Specimen 1 was the whole side surface, while on the others the DIC cameras just focused on the region under pure bending (Figures 4 and 5). Meanwhile, two electric

resistance wire concrete strain gauges were affixed to measure point strain. As shown in Figure 5, one gauge is 20mm away from the top of the beam, and the other is 20mm away from the top of the notch. In addition, a displacement transducer was arranged beneath the mid-span of each specimen.

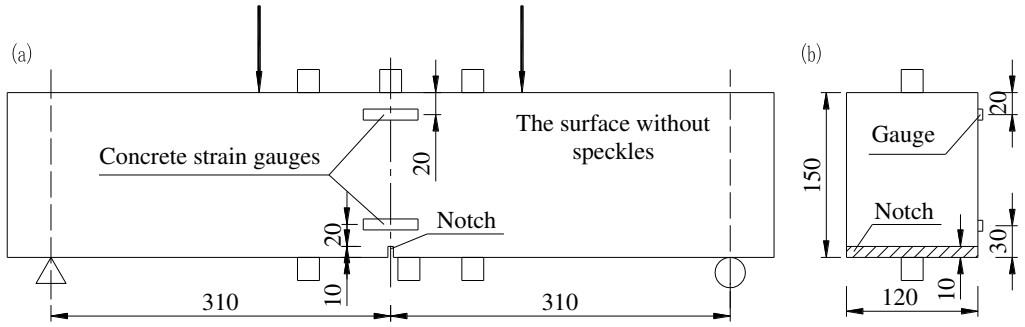

Figure 5. The layout of two concrete strain gauges on each beam: (a) Elevation, (b) The mid-span cross-section diagram (Units in mm).

3.3 Loading conditions

As shown in both Figures 4 and 5, each specimen is subjected to four-point bending. The loads increased monotonically with a rate of 0.005mm/s until one of the following two criteria was satisfied. The first was that a part of the specimen was crushed completely, which led to the failure of the structure, and the other was the loads dropped from peak by 20% or greater.

4 Results

In this Section, data obtained on Beam 1 are discussed extensively to examine the AE activity across the depth of the beam. Meanwhile, some data of the other specimens are also presented herein for the purpose of cross checks. Furthermore, several details are explained as follows prior to further data analysis.

Data acquired just in a specific region on each specimen and in some stages during testing are discussed in the following parts. More specifically, the volume surrounded by all six AE sensors are treated as one "single" section, and just AE signals from it are analysed. Namely, AE events whose x- and y-coordinates satisfy 235mm$\leqslant$x$\leqslant$385mm and 0$\leqslant$y$\leqslant$155mm (for Beams 1, 4, 5 and 6) or 0$\leqslant$y$\leqslant$150mm (only for Beams 2 and 3) are considered hereafter, referring to Figure 4 for the coordinate definition. The reasons are as follows. Firstly, in practice, it is impossible to acquire AE signals from a real cross section. Secondly, the volume, with a length equal to only the beam depth (Figure 4), is very short, and all cross sections in the volume are subjected to bending moment of the same magnitude. Simultaneously, the following analyses focus on processing AE signals recorded during some typical stages and states of every RC beam. The reason lies in that they indicate significant changes in cracks and decrements in stiffness or load bearing capacity of the structure.

208 Three AE descriptors, namely AE event intensity, absolute energy and signal
209 strength, were used in this study. In addition, strain and stress levels of specimens are
210 estimated based on the measurements provided by the two concrete strain gauges and
211 the DIC system. Furthermore, strain diagrams are calculated using the curve-fitting
212 approach and stress diagrams are obtained by combining the stress-strain relation of the
213 concrete material[32] with the strain estimations.

214 ***4.1 Typical loading stages and structural states of RC beams***

215 The failure of Beam 1, i.e. a three-stage loading process, is detailed as follows. In the
216 first stage, no cracks were observed, and the stiffness of the beam was of the greatest
217 magnitude. Theoretically, all parts of each cross section are effective in resisting
218 external moment, and concrete stress is proportional to strain. The stage corresponds to
219 *I-Ia* in the first panel of Figure 6. In the second stage, cracks appeared in the tensile
220 zone very close to the notch, and the deflection of the beam increased significantly,
221 meaning its stiffness also appreciably declined. In theory, the stress increases with strain
222 nonlinearly, and to a cracked section, only a part of the section provides resistance to the
223 bending moment. The second stage corresponds to *II-IIa* in Figure 6. In the third stage,
224 many cracks appeared in both the tensile and compressive regions; and strain increased
225 rapidly until the bearing capacity of the beam was reached; simultaneously, tensile

226 reinforcement yielded. More importantly, the stiffness dramatically reduced. Finally, a
227 part of the concrete in the compressive region was crushed, and then the beam
228 completely failed (See the lower panel of the figure). The last stage corresponds to
229 *III-IIIa* in Figure 6.
230

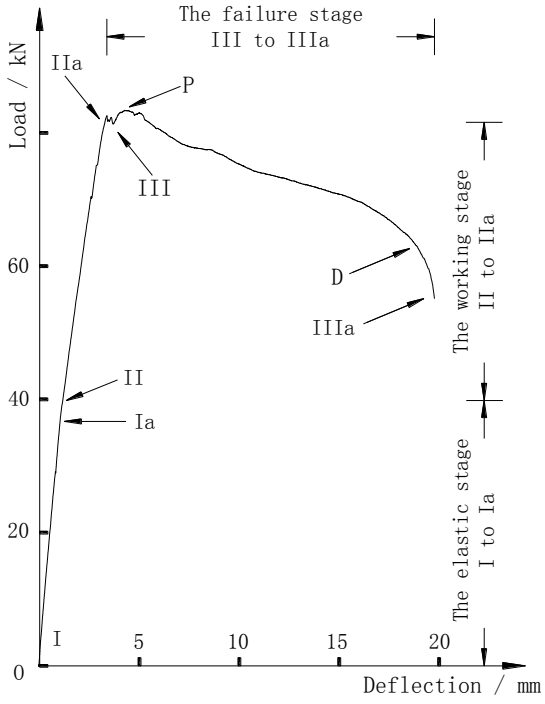

231

Figure 6 The load-deflection curve (Upper) and the failure shape (Lower) of Beam 1.

The above description regarding the failure of Beam 1 is in line with established research [34, 37-39]. Testing of RC beam structures can be divided into several important stages, and these stages can be identified on a load vs. deflection curve, such as the upper panel of Figure 6. Accordingly, all critical stages studied in subsequent parts are listed in Table 3. More importantly, their significance in structural respects is also introduced briefly. Additionally, several critical states listed in Table 3 and Figure 6 are also investigated later.

Table 3. Critical stages and states of a typical RC beam loaded to failure.

Stages / states	Structural significance	Notations
The elastic stage	No crack develops, and the beam behaves elastically.	*I* to *Ia*
The working stage	Cracks develop in tensile regions, and the stiffness therefore decreases slightly.	*II* to *IIa*
The failure stage	Cracks also appear in compressive regions. Reinforcement yields. The bearing capacity and	*III* to *IIIa*

	stiffness decline significantly.	
Yielding of reinforcement	The reinforcement in tension yields	*Ia* to *II*
Peak load	The beam reaches its ultimate bearing capacity.	***III*** to *P*
Load decline	The bearing capacity decreases rapidly.	*P* to *D*

When results are presented as follows, two approaches are employed. The first is to show the AE response in a specific stage. The second is to assess data acquired from the start of the test until the end of the current loading stage, namely the accumulated data.

4.2 In the elastic stage of RC beams

Figure 7 shows the AE data of Beam 1 obtained in the elastic stage and during the period from *Ia* to *II*. Note that the y-axis of all figures is the depth of RC beam section. The cross-sectional height (155mm) is divided into 31 intervals, and three variables, i.e. the AE events, absolute energy and signal strength, are related to each interval (5mm high). When an event is located in an interval, the AE event amount variable increases by one, and the quantities of the energy and the signal strength are added to the other two variables, respectively. The x-coordinate is the amount of AE events (proportion to the intensity), absolute energy or signal strength. Note that the total number of events identified is 3,649, and the order of magnitude of the AE absolute energy and the signal strength in the failure state of Beam 1 is 10^8.

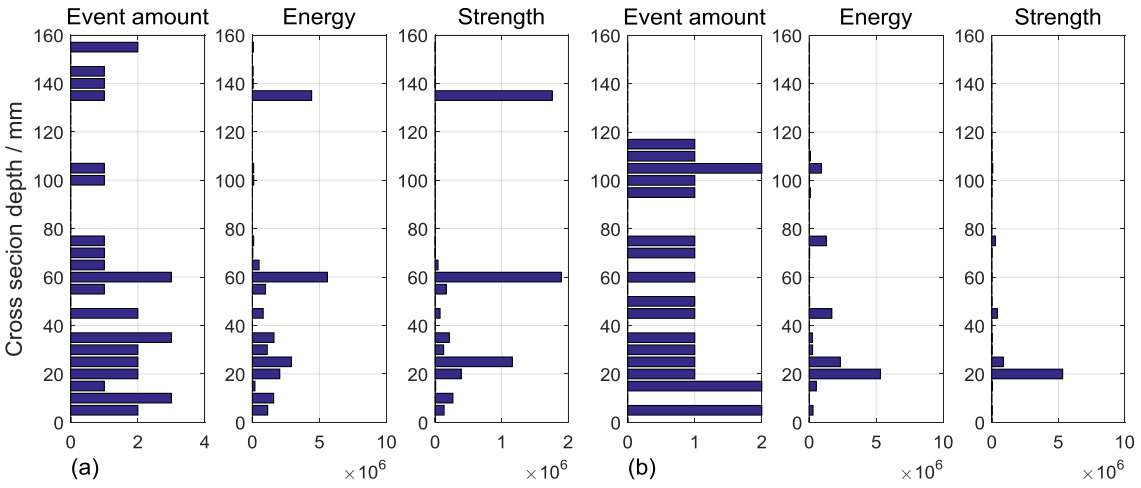

Figure 7 The distributions of the acoustic emissions acquired (a) in the elastic stage and (b) during the onset of the first crack in the tensile area, across the depth of Beam 1 (Energy refers to the AE Absolute Energy, in aJ (attojoules); Strength is short for the Signal Strength, in pVs (picovolt-seconds)).

As shown in the left panel of Figure 7, there are 31 AE events acquired within the elastic stage of loading. The number is less than 1% of the total event amount (3,649), demonstrating AE activity is very low. Furthermore, structural responses of the beam can give deep insight into the characteristic of showing low AE activity at this stage. Since the maximum tensile stress in the concrete is smaller than the modulus of rupture at this stage, all parts of a concrete section are effective in resisting stress which is proportional to strain[34, 37-39]. Namely, the beam is behaving elastically. Theoretically, it is therefore, generally assumed that no damage has occurred [40]. Consequently, the AE activity inside the beam is very low. In conclusion, the structural

responses come to a very good agreement with the AE detected.

The first crack appeared during the period from *Ia* to *II* in Figure 6, and Figure 7 shows the corresponding AE measurements. The second panel of Figure 7 reveals that 19 AE events were recorded, similar to what happened in the previous stage. Therefore, the AE activity in this period is also considered to be considerably low. However, as shown in the load vs. deflection curve (Figure 6), the slope of the curve in the post-elastic stage decreases slightly, meaning that the stiffness has reduced. For comparison, the data from the same stage of testing in Beam 3 is shown in Figure 8 and support the the above conclusions.

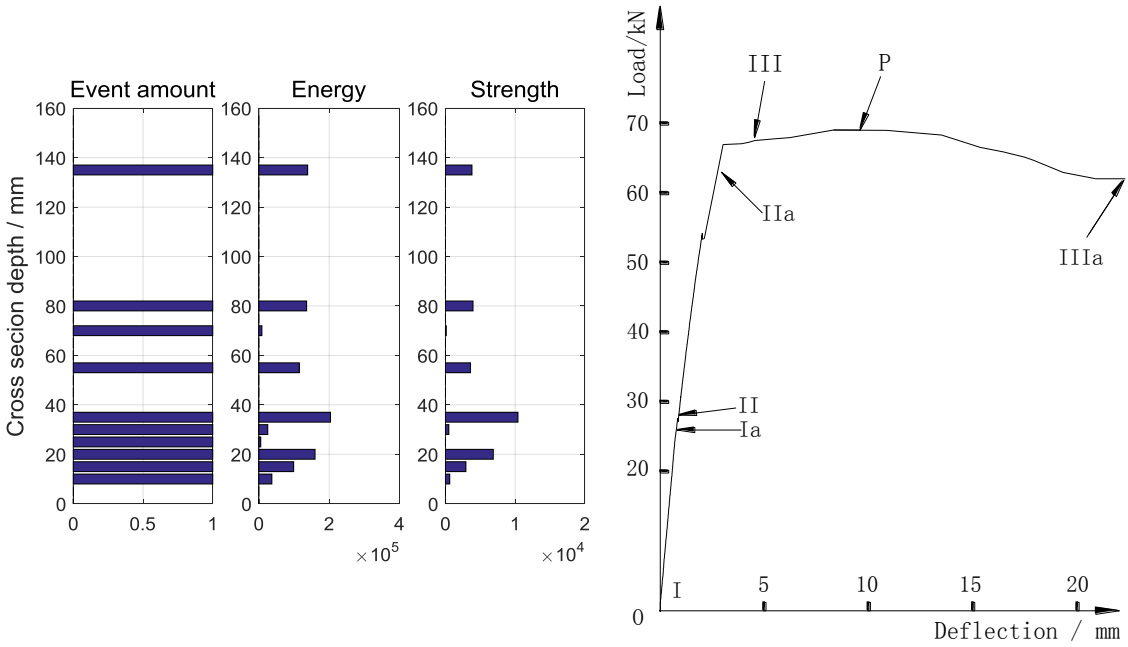

Figure 8 The distributions of the acoustic emissions acquired in the elastic stage through the depth (Left) and the load-deflection curve (Right) of Beam 3

4.3 In the working stage of RC beams

As shown in Figure 9, two features are considerably obvious at this stage. Firstly, 211 events, 581% larger than the amount of emissions captured in the elastic stage, were acquired on Beam 1, meaning that the AE activity significantly increased. However, the activity is still low as it represents only 5.78% of the total number of the events captured in the entire test. Secondly, most of the events took place in the tensile zone of the beam, meaning the AE event distribution roughly matched with that of the tensile stress (the right panel in Figure 9). Meanwhile, the intensity of AE events in the compressive region also rose. In addition, analysing the data of the AE absolute energy came to similar conclusions, and the same characteristics were also found on the other specimens, which are not presented here to save space.

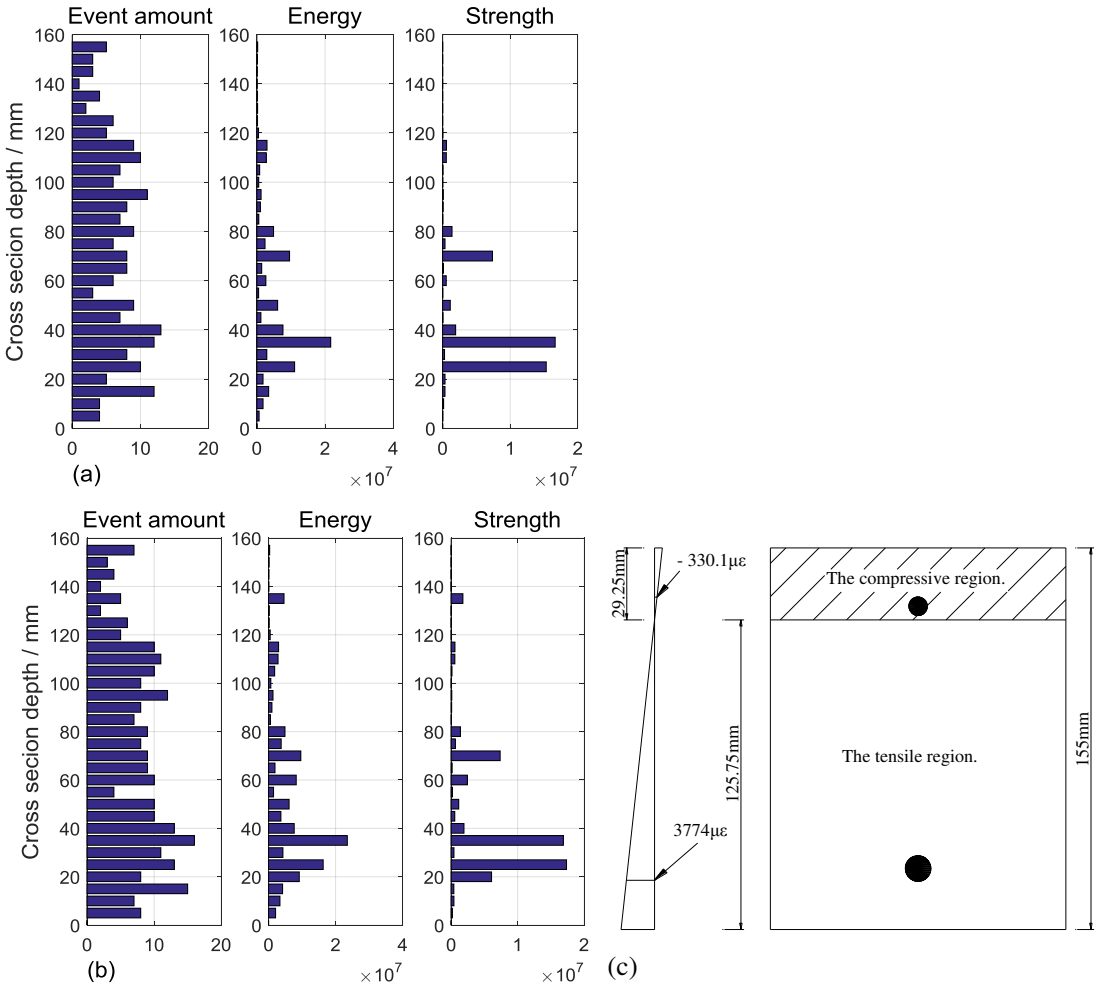

Figure 9 The distributions of the acoustic emissions acquired (a) in the working stage, (b) until the end of the stage and (c) the corresponding total strain distribution through the depth of Beam 1.

4.4 In the failure state of RC beams

For Beam 1, more than 90% AE events were captured in the failure stage; therefore, it is quite clear that the beam was very active in terms of AE. Meanwhile, several crucial events, e.g. the yielding of reinforcement and the reaching of peak loads, occurred

312 during this stage. Hence, the stage is analysed carefully as follows.

313 In Figure 10, all AE and DIC data acquired in the failure stage (Panel (a)) and
314 throughout the test (Panels (b) and (c)) are presented, while further analysis on the
315 corresponding behaviour of Beam 1 is shown in Figure 11. On the whole, Figure 10
316 shows two features. Firstly, the AE activity dramatically rises in the stage. For example,
317 as shown in Panels (a) and (b), the order of magnitude of the AE absolute energy and
318 signal strength is 10^8, while it is 10^7 in the previous stage. Secondly, the AE event
319 intensity in the compressive zone is far greater than that in the tensile region. Both
320 features are also observed on other specimens, such as Beam 4 (Figure 12). Additionally,
321 other researchers [19] also came to the same conclusion, namely overwhelming majority
322 of AE events appear during the final failure of structures.
323

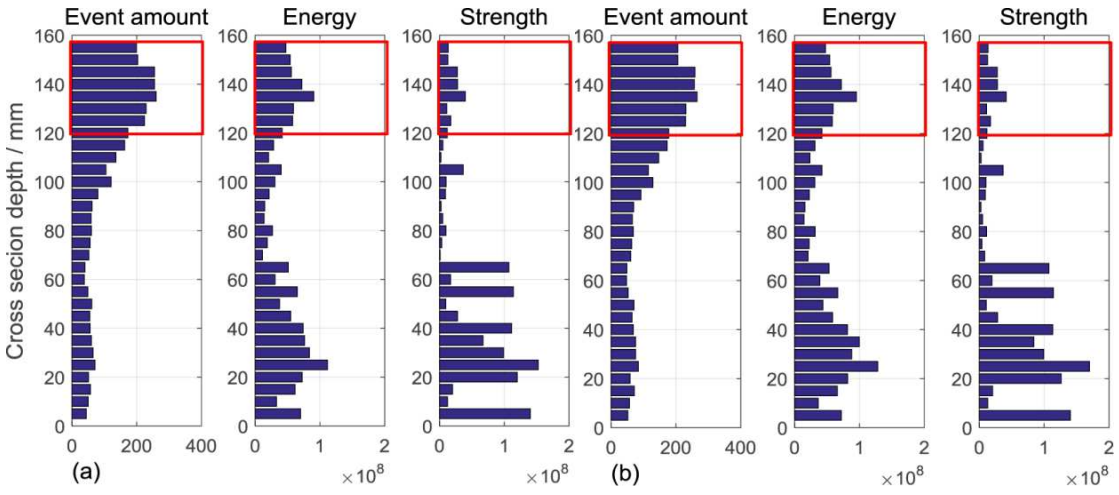

324

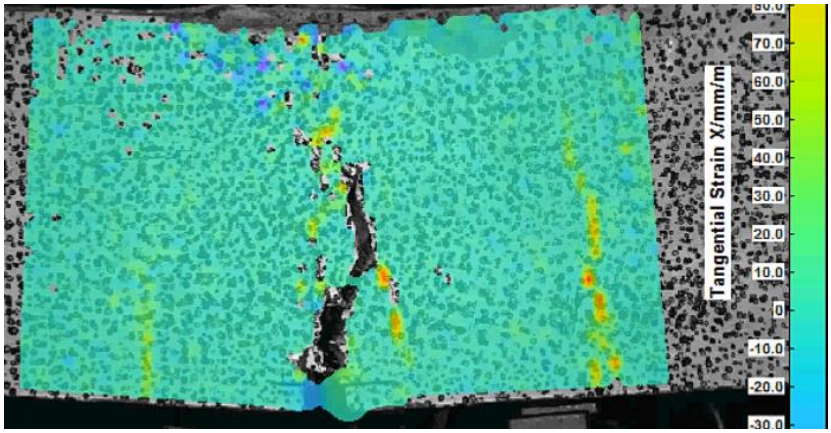

Figure 10 The distributions of the acoustic emissions acquired (a) in the failure stage, (b) until the end of the test and (c) the corresponding total strain distribution through the depth of Beam 1(The compressive concrete zone is circled with red rectangles).

More importantly, an insight into the AE results comes from the examination of the correlation between the AE event intensity distribution and that of the stress in the compressive zone (Figure 11). To analyse the correlation, the following three steps are needed. Firstly, in Panel (a), the strain over the mid-span section of Beam 1 is calculated according to the data (Figure 10(c)) obtained with the DIC device in the ultimate state. Secondly, in Panel (b), the stress in the compressive zone is calculated according to the stress-strain relation (Eq. (1)) [34].

$$\frac{\sigma_c}{f_{cm}} = \frac{k\eta - \eta^2}{1 + (k-2)\eta} \tag{1}$$

$$\eta = \frac{\varepsilon_c}{\varepsilon_{c1}}, \quad \varepsilon_c \le 0.0035, \quad k = \frac{1.05E_{cm} \times |\varepsilon_{c1}|}{f_{cm}}$$

where σ_c is the compressive stress value when strain is $\varepsilon_c(\leq 0.0035)$, and ε_{c1} is the strain at peak stress. f_{cm} and E_{cm} are the mean compressive strength at 28 days and the modulus of elasticity, respectively. ε_{c1}, f_{cm} and E_{cm} are specified in the code[34]. Note that only the compressive stress is considered here, because the concrete in the tensile zone has been cracked due to vulnerability of the material [41]. Finally, the distribution of the AE through the depth of the compressive zone is estimated using the curve-fitting approach (Panel (c)). Note that in Panel (b), there is a blank (14mm high) on the top of the section. This attributes to the excessive strain over the region. Eq. (1) is just applied to cases where $\varepsilon_c \leq 0.0035$ (Figure 1(b)), however, ε_c in the blank region does not satisfy the condition. Hence, the stress over the region cannot be computed according to Eq.(1). In fact, $\varepsilon_c > 0.0035$ means that, physically, concrete has been crushed. Additionally, the blank is confirmed in Figure 15 and is discussed in Section 6 again.

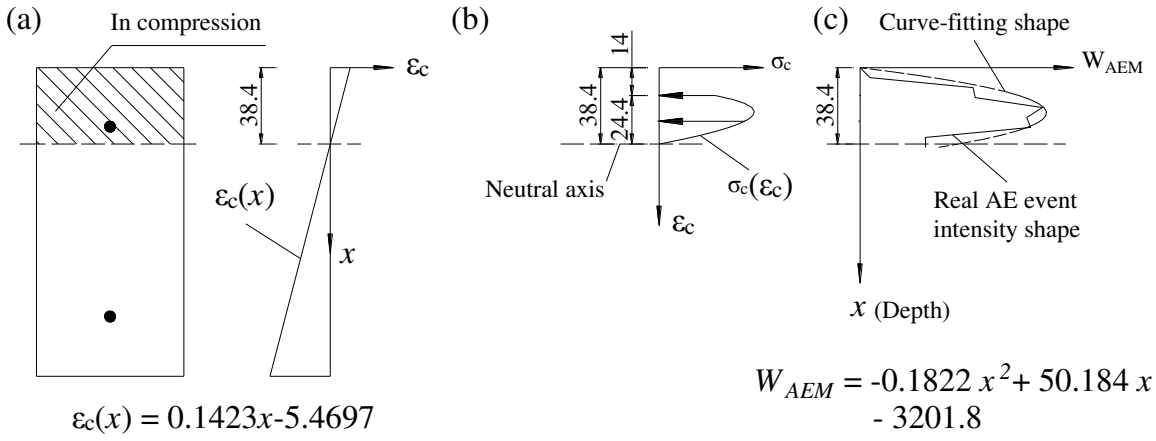

Figure 11 (a) The strain diagram on the mid-span section, (b) the corresponding stress distribution and (c) the AE event intensity distribution in the compressive region of Beam 1 (Length in mm, stress and strength in MPa).

As shown in Panels (b) and (c) of Figure 11, the distribution of the AE event intensity correlates very well with that of the compressive stress over the zone. Firstly, these two distributions are of very similar curve shapes. Secondly, the peak values of the AE event intensity and the stress occur at almost the same location. More specifically, the former appears 20mm away from the top, the latter 22mm. This was consistent in all beams and demonstrated by Figure 12 from Beam 4. In conclusion, the AE intensity variation pattern accurately correlates with the distribution of the compressive stress through the cross-sectional depth in the failure stage.

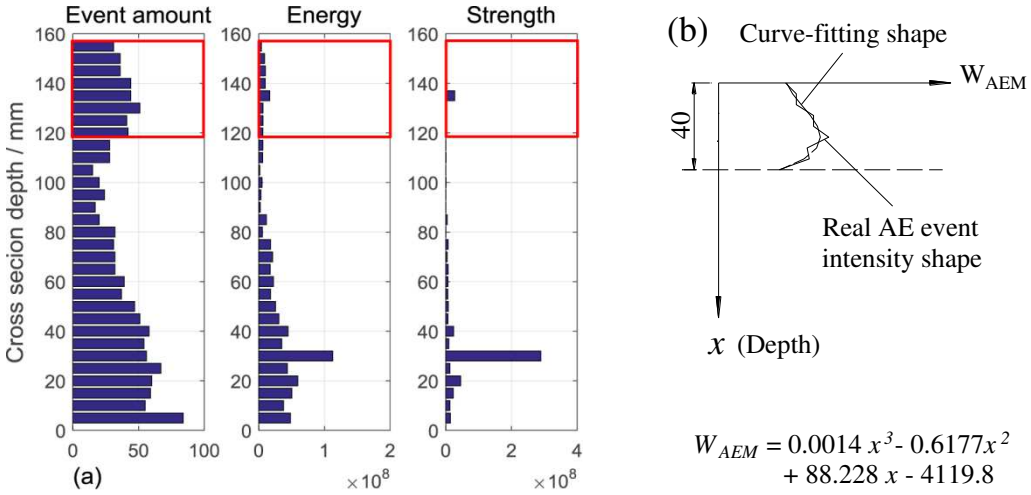

Figure 12 (a) The distribution of the acoustic emissions acquired in the test on Beam 4 through the depth and (b) the AE event intensity distribution over the compressive region circled with red rectangles (Length in mm).

Three critical issues, i.e. the yielding of reinforced steel bars, the peak loads and the decrease of the load, occurred during the failure stage, and they deserve further investigation. The AE data corresponding to the first two sub stages are illustrated in Figure 13. The figure shows that, compared with the AE response in the working stage, the AE activity does not increase significantly. More specifically, the AE event intensity remains at the same level, and the order of magnitude of the absolute energy and signal strength remains unchanged. However, the activity in the compressive zone begins to rise although it is still lower than that in the tensile region. In conclusion, the significant changes in AE activity shown in Figure 10 do not occur in these two periods of time.

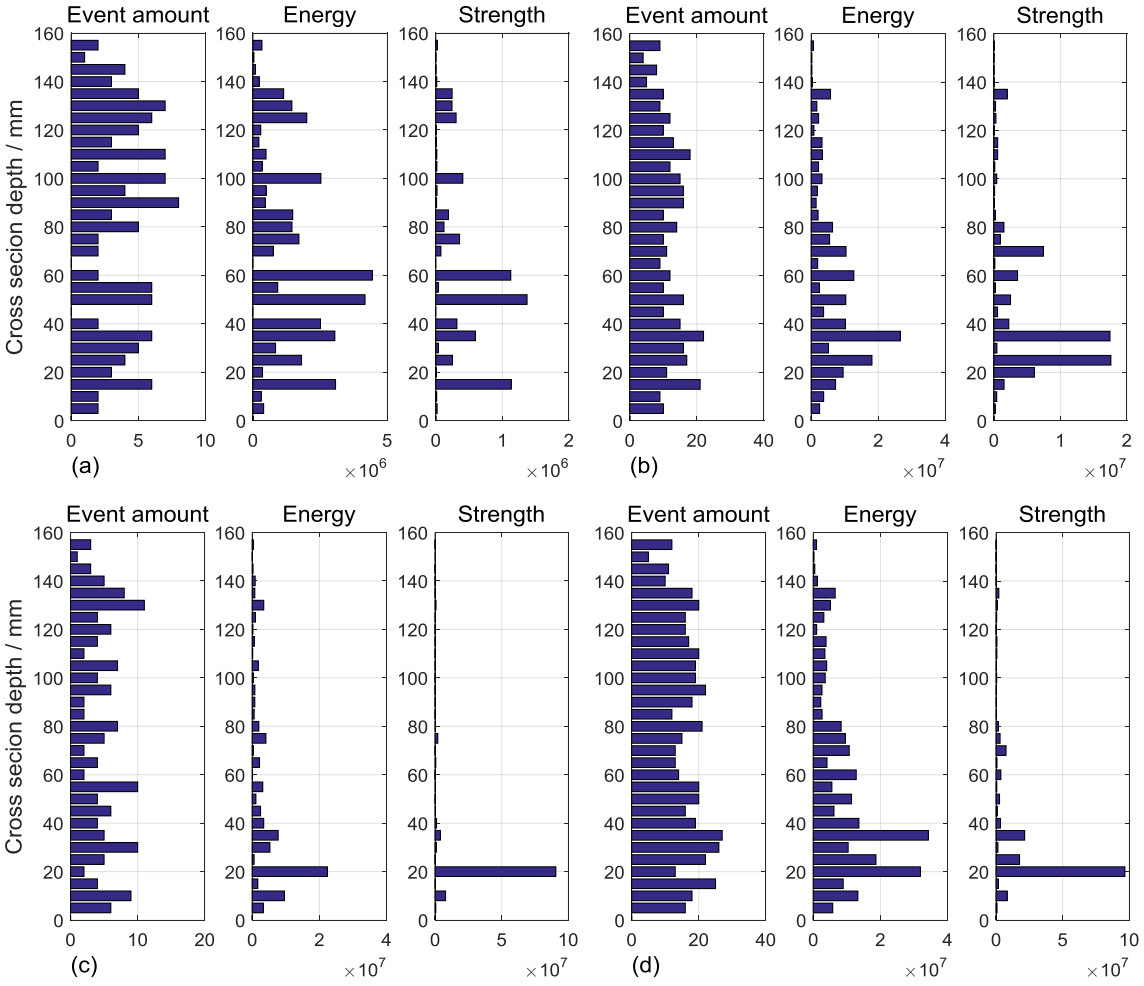

Figure 13 The distributions of the acoustic emissions acquired (a) during the yielding of reinforcement, (b) until the yielding of reinforcement, (c) during the period from III to P and (d) until the peak load, namely Point P, through the depth of Beam 1.

In fact, as shown in Figure 14, the beam experiences a dramatic increase in the AE response when the loads drop from peak and the beam reaches ultimate failure. 82.85% of all AE events occur in the duration. Furthermore, as showed in Panel (c), the shape of the AE event intensity distribution curve closely matches the stress diagram (Figure

11(b)). Meanwhile, compared with the situations in the previous stages, the order of magnitude of the AE absolute energy and the signal strength rises from 10^7 to 10^8. Accordingly, these data mean that Beam 1 shows the highest AE activity in this period.

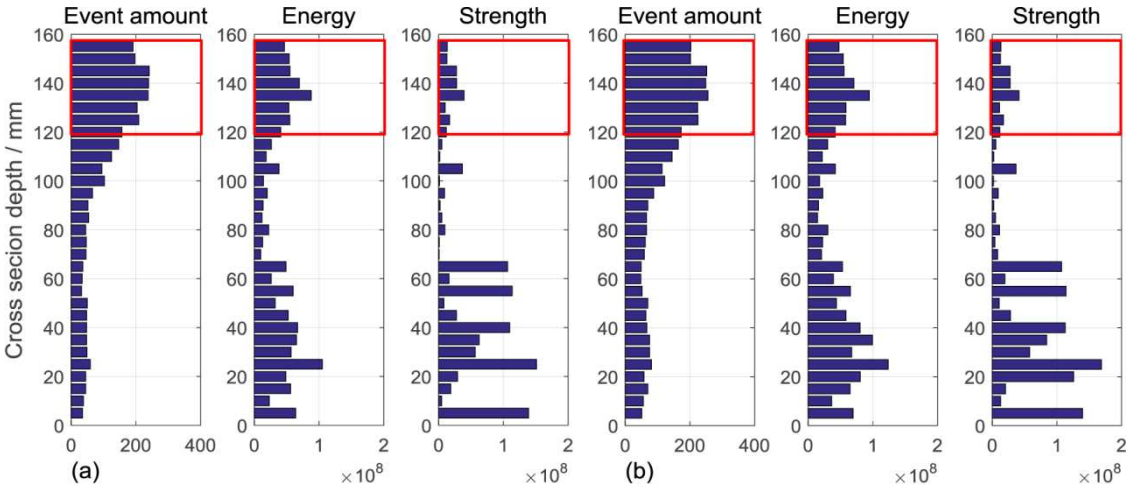

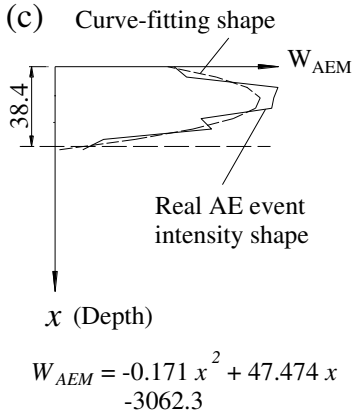

$$W_{AEM} = -0.171\,x^2 + 47.474\,x - 3062.3$$

Figure 14 The distributions of the acoustic emissions acquired (a) during the period from P to D, (b) until the Point D across the depth of Beam 1 and (c) the AE event intensity distribution over the compressive region circled with red rectangles (Length in mm).

405 ## 5 Discussions

406 ### *5.1 Observations from cut cross sections*

407 Beams 5 and 6 were cut at the failed sections after final failure. As shown in Figure 15,
408 two conclusions can be drawn based on observations from the cut sections. Firstly, the
409 thickness of the crushed concrete measured in Figure 15 matches with the estimation
410 (14mm high) in Figure 11(b). In the discussion regarding the zero-stress zone in Figure
411 11(b), it was theoretically concluded that the concrete on the top of the section was
412 crushed, which resulted in the 14mm-depth interval with zero stress. It is confirmed
413 here, and the thickness of the crushed concrete measured in Figure 15, ranging from
414 13mm to 20mm (the space in between the two pairs of red dashed lines), matches very
415 well with the estimation (14mm). Secondly, AE events occurred through the whole
416 depth. This conclusion is supported by the observation that cracks developed during
417 testing had penetrated through almost the entire cross section. This is very strong
418 evidence of the AE distributions shown in Figures 9, 10, 12, and 13. In conclusion,
419 these observations strongly support the outputs discussed previously.
420

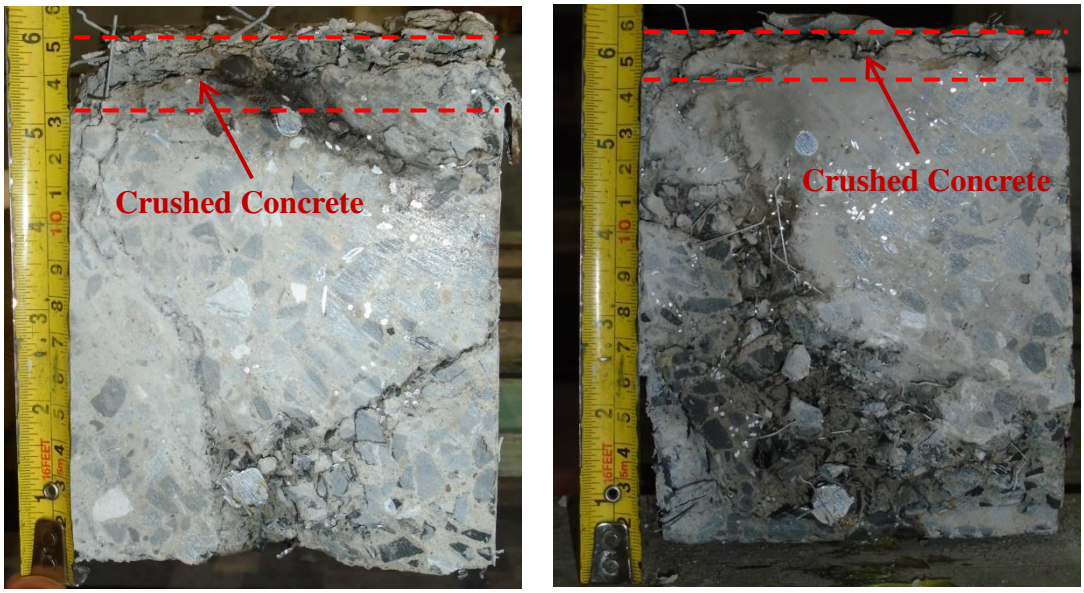

Figure 15 The cut cross sections of Beams 5 (Left) and 6, respectively.

5.2 AE on the specimen that failed in the shear mode

Only Beam 2 failed in the shear mode (See Table 1 and Figure 16). The AE variation across the depth of the beam is distinctively different from those that failed in the flexural mode. Firstly, as shown in the left panel in Figure 16, the amount of AE events acquired in the compressive region is far less than that from the tensile area. The lower activity in the compressive region of Beam 2 means that the damage level is relatively low, suggesting the stress level of the beam is also low. More importantly, this indicates that the strength potential of the concrete is not fully used due to the occurrence of the shear failure. Secondly, the AE absolute energy and the signal strength of Beam 2 are at least one order of magnitude smaller than that of the other specimens. As shown in

Figures 10, 11 and 14, on Beam 2, the order of magnitude is 10^7 or 10^6, while that of beams failed in the flexural mode is 10^8. This also indicates the material in Beam 2 is not completely utilised, and the conclusion matches with findings in traditional concrete structure research [38, 39].

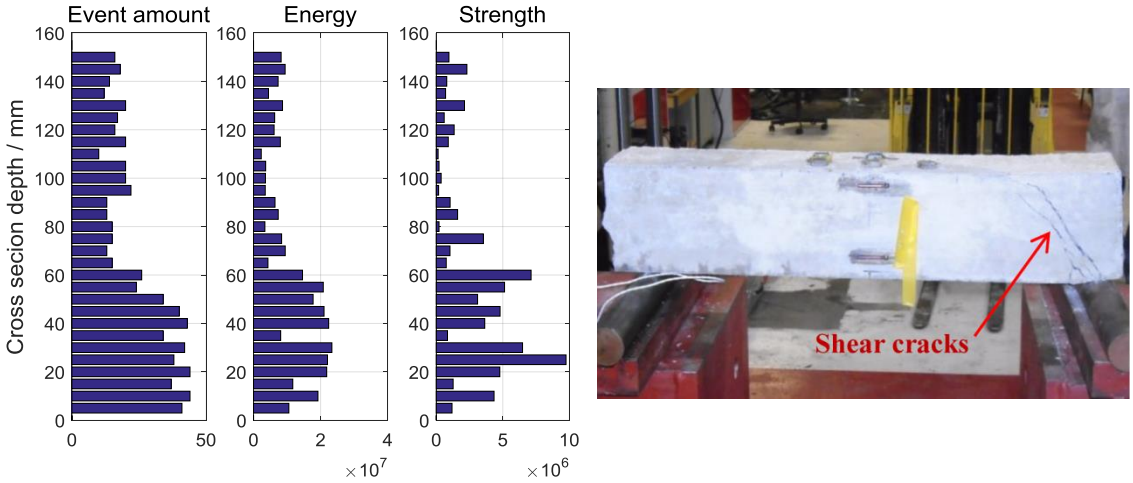

Figure 16 The distribution of the AE acquired through the test on Beam 2 (Left) and the shape when it failed (Right).

6 Conclusions

This study focused on AE distribution through the depth of an RC beam and the correlation between AE and stress variations. Experiments on six beams were conducted, and all critical stages of these beams, i.e. the elastic stage, the working stage and the failure stage, were examined carefully. AE response, structural deflections and strain/stress were measured and then analysed in detail. Based on this work, the

following conclusions were drawn:

- AE is highly capable of characterising the behaviours through the depth of RC beams. Furthermore, the AE event intensity outperformed the absolute energy and the signal strength in the study.
- In the elastic stage, the AE activity was very low. For example, less than 1% of the total amount of AE events were acquired on Beam 1, and the order of magnitude of both the AE absolute energy and the signal strength was 10^6 (Figure 7).
- In the working stage, the AE activity rose slightly, however, it was not yet very high. More specifically, only about 5% of the total AE events were recorded. The order of magnitude of the absolute energy/signal strength was 10^7 (Figure 9). Meanwhile, the AE response distribution matched with that of the stress distribution.
- In the failure stage, the overwhelming majority of AE were captured, meaning that specimens were considerably active. More than 90% of the total AE events were recorded, and the order of magnitude for energy was 10^8 (Figure 10). Nevertheless, the beam was relatively inactive during yielding of reinforcement

and at peak load (Figure 13). However, the AE was highly active when the loads dropped from peak (Figure 14).

- The most significant finding in the study is that the distribution of the AE event intensity accurately matches with that of the stress over the compressive zone. (Figures 11, 12 and 14). Namely, the pattern of AE event intensity distribution in the depth direction is very similar to the compressive stress diagram. Meanwhile, the peak of the AE event intensity and the stress appears at almost the same location.

The above conclusions suggest that the AE technology is of great potential to serve as a measure to estimate critical stress levels of RC beam structures. This topic is addressed in another article. Note that the idea, determining critical stress states in structures via AE parameter distribution analysis, deserves researchers and practisers' more work to extend it to more scenarios and inspire more innovations.

Funding

This work was funded by the Open Fund of State Key Laboratory Breeding Base of Mountain Bridge and Tunnel Engineering (Chongqing Jiao tong University) and Key Laboratory of Bridge Structure Engineering Transportation Industry (Chongqing) (CQSLBF-Y15-2), National Natural Science Foundation of China (51508058, 51479013), Youth Science and Technology Talent Cultivating Plan of Chongqing City (cstc2014kjrc-qnrc30001).

Acknowledgement

The authors highly appreciate the contributions from technicians, Carl Wadsworth, Ian King, Jack Morgan and Richard Thomas; faculty members, John McCrory, Davide Crivelli and Ryan Marks; Ph.D. candidates, ZAC (王宇) and Stephen Grigg in Cardiff School of Engineering, Cardiff University, Wales, United Kingdom.

References

[1] N.M. Nor, A. Ibrahim, N.M. Bunnori, H.M. Saman, S.N.M. Saliah, S. Shahidan, Diagnostic of fatigue damage severity on reinforced concrete beam using acoustic emission technique, Engineering Failure Analysis 41(5) (2014) 1-9.

[2] Z. Liu, P.H. Ziehl, Evaluation of Reinforced Concrete Beam Specimens with Acoustic Emission and Cyclic Load Test Methods, Aci Structural Journal 106(3) (2009) 288-299.

[3] M.A.A. Aldahdooh, N.M. Bunnori, Crack classification in reinforced concrete beams with varying thicknesses by mean of acoustic emission signal features, Construction & Building Materials 45(45) (2013) 282–288.

[4] M.A.A. Aldahdooh, N.M. Bunnori, M.A.M. Johari, Damage evaluation of reinforced concrete beams with varying thickness using the acoustic emission technique, Construction & Building Materials 44(44) (2013) 812-821.

[5] S. Hu, J. Lu, F. Xiao, Evaluation of concrete fracture procedure based on acoustic emission parameters, Construction & Building Materials 47(47) (2013) 1249-1256.

[6] N.M. Nor, A. Ibrahim, N.M. Bunnori, H.M. Saman, Acoustic emission signal for fatigue crack classification on reinforced concrete beam, Construction & Building Materials 49(6) (2013) 583-590.

[7] S. Shahidan, R. Pulin, N.M. Bunnori, K.M. Holford, Damage classification in reinforced concrete beam by acoustic emission signal analysis, Construction & Building Materials 45(13) (2013) 78–86.

[8] P.H. Ziehl, Early corrosion monitoring of prestressed concrete piles using acoustic emission, Spie Smart Structures & Materials + Nondestructive Evaluation & Health Monitoring, 2013, pp. 869407-869407-11.

[9] M. Abdelrahman, M.K. Elbatanouny, P.H. Ziehl, Acoustic emission based damage assessment method for prestressed concrete structures: Modified index of damage, Engineering Structures 60(60) (2014) 258-264.

[10] W. Vélez, F. Matta, P. Ziehl, Acoustic emission monitoring of early corrosion in prestressed concrete piles, Structural Control & Health Monitoring 22(1) (2014) 873–887.

[11] R. Anay, T.M. Cortez, D.V. Jáuregui, M.K. Elbatanouny, P. Ziehl, On-Site Acoustic Emission Monitoring for Assessment of a Prestressed Concrete Double-Tee-Beam Bridge without Plans, Journal of

519 Performance of Constructed Facilities 04015062 (2015) 1-9.
520 [12] R.S. Gostautas, G. Ramirez, R.J. Peterman, D. Meggers, Acoustic Emission Monitoring and Analysis of
521 Glass Fiber-Reinforced Composites Bridge Decks, Journal of Bridge Engineering 10(6) (2005) 713-721.
522 [13] S. Degala, P. Rizzo, K. Ramanathan, K.A. Harries, Acoustic emission monitoring of CFRP reinforced
523 concrete slabs, Construction & Building Materials 23(5) (2009) 2016-2026.
524 [14] H.D. Yun, W.C. Choi, S.Y. Seo, Acoustic emission activities and damage evaluation of reinforced
525 concrete beams strengthened with CFRP sheets, Ndt & E International 43(7) (2010) 615-628.
526 [15] W.C. Choi, H.D. Yun, Acoustic emission activity of CFRP-strengthened reinforced concrete beams
527 after freeze–thaw cycling, Cold Regions Science & Technology 110 (2014) 47-58.
528 [16] A. Nair, C.S. Cai, F. Pan, X. Kong, Acoustic emission monitoring of damage progression in CFRP
529 retrofitted RC beams, 1(1) (2014) 111-130.
530 [17] E. Selman, A. Ghiami, N. Alver, Study of fracture evolution in FRP-strengthened reinforced concrete
531 beam under cyclic load by acoustic emission technique: An integrated mechanical-acoustic energy
532 approach, Construction & Building Materials 95 (2015) 832-841.
533 [18] P.R. Prem, A.R. Murthy, Acoustic emission and flexural behaviour of RC beams strengthened with
534 UHPC overlay, Construction & Building Materials 123(1) (2016) 481-492.
535 [19] S. Rouchier, G. Foray, N. Godin, M. Woloszyn, J.J. Roux, Damage monitoring in fibre reinforced
536 mortar by combined digital image correlation and acoustic emission, Construction & Building Materials
537 38(38) (2013) 371–380.
538 [20] M.K. Elbatanouny, P.H. Ziehl, A. Larosche, J. Mangual, F. Matta, A. Nanni, Acoustic emission
539 monitoring for assessment of prestressed concrete beams, Construction & Building Materials 58(58)
540 (2014) 46-53.
541 [21] M. Ohtsu, K. Mori, Y. Kawasaki, Corrosion Process and Mechanisms of Corrosion-Induced Cracks in
542 Reinforced Concrete identified by AE Analysis, Strain 47(s2) (2011) 179–186.
543 [22] J.H. Kurz, New approaches for automatic threedimensional source localization of acoustic
544 emissions--Applications to concrete specimens, Ultrasonics 63 (2015) 155-162.
545 [23] V. Janapati, F. Kopsaftopoulos, F. Li, J.L. Sang, F.K. Chang, Damage Detection Sensitivity
546 Characterization of Acousto-Ultrasound-based SHM Techniques, Structural Health Monitoring 15(2)
547 (2016) 143-161.
548 [24] R.V. Sagar, B.K.R. Prasad, R.K. Singh, Kaiser effect observation in reinforced concrete structures and
549 its use for damage assessment, Archives of Civil & Mechanical Engineering 15(2) (2014) 548-557.
550 [25] X. Fu, Q. Xie, L. Liang, Comparison of the Kaiser effect in marble under tensile stresses between the
551 Brazilian and bending tests, Bull. Eng. Geol. Environ. 74(2) (2015) 535-543.
552 [26] A. Lehtonen, J.W. Cosgrove, J.A. Hudson, E. Johansson, An examination of in situ rock stress
553 estimation using the Kaiser effect, Eng. Geol. 124 (2012) 24-37.

554 [27] E. Tuncay, Y. Obara, Comparison of stresses obtained from Acoustic Emission and Compact
555 Conical-Ended Borehole Overcoring techniques and an evaluation of the Kaiser Effect level, Bull. Eng.
556 Geol. Environ. 71(2) (2012) 367-377.
557 [28] K. Komloš, S. Popovics, T. Nürnbergerová, B. Babál, J.S. Popovics, Ultrasonic pulse velocity test of
558 concrete properties as specified in various standards, Cement & Concrete Composites 18(5) (1996)
559 357-364.
560 [29] C. Grosse, H. Reinhardt, T. Dahm, Localization and classification of fracture types in concrete with
561 quantitative acoustic emission measurement techniques, Ndt & E International 30(4) (1997) 223-230.
562 [30] D.G. Aggelis, T. Shiotani, Repair evaluation of concrete cracks using surface and
563 through-transmission wave measurements, Cement & Concrete Composites 29(9) (2007) 700-711.
564 [31] S. Momoki, T. Shiotani, H.K. Chai, D.G. Aggelis, Y. Kobayashi, Large-scale evaluation of concrete
565 repair by three-dimensional elastic-wave-based visualization technique, Structural Health Monitoring
566 12(3) (2013) 240-251.
567 [32] G. Karaiskos, E. Tsangouri, D.G. Aggelis, K. Van Tittelboom, N. De Belie, D. Van Hemelrijck,
568 Performance monitoring of large-scale autonomously healed concrete beams under four-point bending
569 through multiple non-destructive testing methods, Smart Materials & Structures 25(5) (2016) 055003.
570 [33] M. Ohtsu, Elastic wave methods for NDE in concrete based on generalized theory of acoustic
571 emission, Construction & Building Materials 122 (2016) 845-854.
572 [34] Partie, EUROCODE 2: DESIGN OF CONCRETE STRUCTURES. PART 1-1. GENERAL RULES AND RULES
573 FOR BUILDINGS 2004.
574 [35] G. Swit, Diagnostics of Prestressed Concrete Structures by Means of Acoustic Emission, The
575 Proceedings of 2009 International Conference on Reliability,maintainability and Safety, 2009, pp.
576 958-962.
577 [36] M.G.R. Sause, Investigation of Pencil-Lead Breaks as Acoustic Emission Sources, Journal of Acoustic
578 Emission 29(1) (2011) 184-196.
579 [37] A.H. Mattock, L.B. Kriz, E. Hognestad, Rectangular concrete stress distribution in ultimate strength
580 design.
581 [38] S.Y. Debaiky, E.I. Elniema, BEHAVIOR AND STRENGTH OF REINFORCED CONCRETE HAUNCHED BEAMS
582 IN SHEAR, Journal of the American Concrete Institute (1982).
583 [39] A.A. Committee, The shear strength of reinforced concrete members—slabs, Journal of the
584 Structural Division 99 (1973) 1091-1187.
585 [40] S. Liu, L. Zhang, Z. Chen, J. Zhou, C. Zhu, Mode-specific damage identification method for reinforced
586 concrete beams: Concept, theory and experiments, Construction & Building Materials 124 (2016)
587 1090-1099.
588 [41] E. Hognestad, N.W. Hanson, Mchenry, Douglas, Concrete Stress Distribution in Ultimate Strength

589 Design, Journal of the American Concrete Institute (1955).
590